

Communication

# Extending the Photon Energy Coverage of a Seeded Free-Electron Laser via Reverse Taper Enhanced Harmonic Cascade

Kaiqing Zhang , Tao Liu, Zheng Qi, Xiaoxi Fu, Chao Feng \*, Haixiao Deng and Bo Liu

Shanghai Advanced Research Institution, Chinese Academy of Sciences, Shanghai 201210, China; zhangkaiqing@zjlab.org.cn (K.Z.); liutao@zjlab.org.cn (T.L.); qizheng@zjlab.org.cn (Z.Q.); fuxiaoxi@zjlab.org.cn (X.F.); denghaixiao@zjlab.org.cn (H.D.); liubo@zjlab.org.cn (B.L.)

\* Correspondence: fengchao@zjlab.org.cn

**Abstract:** External seeded free-electron lasers (FELs) hold promising prospects for producing intense coherent radiation at high harmonics of a conventional laser. The practical harmonic up-conversion efficiencies of current seeding techniques are limited by various three-dimensional effects on the electron beam. In this paper, a novel method is proposed to extend the wavelength coverage of a seeded FEL by combining the reverse taper undulator with the echo-enabled harmonic generation. The proposed technique can significantly enhance the bunching at ultra-high harmonics and preserve the electron beam qualities from degradation by deleterious effects. Theoretical analysis and numerical simulation are performed, and the results demonstrate that stable, intense, nearly fully coherent FEL pulses with photon energy up to 1 keV can be generated. The proposed technique may open up new opportunities to obtain laser-like pulses at sub-nanometer wavelength.

**Keywords:** free electron laser; reverse taper; seeded FEL; intra beam scattering; synchrotron radiation effects



**Citation:** Zhang, K.; Liu, T.; Qi, Z.; Fu, X.; Feng, C.; Deng, H.; Liu, B. Extending the Photon Energy Coverage of a Seeded Free-Electron Laser via Reverse Taper Enhanced Harmonic Cascade. *Photonics* **2021**, *8*, 44. <https://doi.org/10.3390/photonics8020044>

Received: 6 January 2021

Accepted: 7 February 2021

Published: 9 February 2021

**Publisher's Note:** MDPI stays neutral with regard to jurisdictional claims in published maps and institutional affiliations.



**Copyright:** © 2021 by the authors. Licensee MDPI, Basel, Switzerland. This article is an open access article distributed under the terms and conditions of the Creative Commons Attribution (CC BY) license (<https://creativecommons.org/licenses/by/4.0/>).

## 1. Introduction

The high gain X-ray free electron laser (FEL) opens new chapters to various frontiers of nanoscale scientific applications in biology, chemistry, material science for the abilities to provide femtosecond pulses with gigawatt peak power and tunable wavelength down to less than 0.1 nm. The successful operations of several X-ray FEL facilities indicate a new era of X-ray science, most of which employ the mechanism of self-amplified spontaneous emission (SASE) [1–5]. While SASE FEL holds promising abilities to produce X-ray pulses with great spatial coherence and tunable wavelength, its output has typically limited coherence in the temporal and spectral domains since the initial signal arises from chaotic spontaneous emission with fluctuating temporal structure [6]. Many recently developed or emerging scientific techniques require the femtosecond X-ray pulses with intense peak power, spatial as well as temporal coherence at sub-nanometer wavelength [7–9]. Self-seeding [10–17] is developed to generate full coherent X-ray pulse by implementing an optical monochromator to reduce the bandwidth of the noisy SASE spectrum. However, the intrinsic SASE fluctuation, microbunching instability of the electron beam [16] and the properties of optical monochromator [12,16] might significantly affect the characteristics of self-seeding FEL.

External seeded FELs are developed to provide stable and fully coherent FEL pulses by triggering the amplification process with external conventional lasers at the ultraviolet wavelength. To produce coherent pulses at extreme ultraviolet (EUV)/X-ray range, frequency up-conversion schemes [18–21] are generally required due to the lack of intense and coherent laser sources at short wavelength. Among these external seeded techniques, the recently developed echo-enabled harmonic generation (EEHG) [22–30] has the highest harmonic up-conversion efficiency, holding the capability to generate intense, highly coherent soft X-ray pulses with a wavelength of a few nanometers [30]. Theoretical and numerical

investigations within the framework of idealized models indicate further extension of the coverage of a single EEHG to shorter wavelength is very challenging due to various three-dimensional effects [23,28]. These effects play important roles in the forming process of the fine structure of EEHG and will eventually lead to the damping of bunching at 2 nm and below.

In this paper, we propose a novel technique to extend the photon energy coverage of a single-stage seeded FEL by combining the reverse taper undulator [31–35] with the EEHG. The proposed technique first operates a single-stage EEHG to generate coherent microbunching at a relatively low harmonic. Then a reverse tapered undulator is utilized to enhance the bunching while suppress the growth of energy spread. Further harmonic jump and amplification of the short wavelength radiation are realized in the final radiator. The proposed technique can significantly reduce the difficulties and requirements in implementing external seeding at a sub-nanometer wavelength range.

## 2. Method and Principles

Figure 1 shows the schematic layout of the proposed technique, which extends the photon energy coverage by two frequency up-conversion processes: the first up-conversion process uses a typical single-stage EEHG scheme; the second up-conversion process benefits from the use of reverse tapered undulator, which can amplify the bunching factor at high harmonic but suppress the increase of energy spread [33]. The electron beam from the linac firstly passes through a modified EEHG stage, which consists of two modulator-chicane modules, two seed lasers ( $\lambda_{seed1} = \lambda_{seed2} = \lambda_s$ ) and a reverse tapered undulator resonated at a target harmonic of the seed. The electron beam interacts with the first seed laser to produce a relatively small energy modulation in the first modulator. Then the electron beam passes through a strong magnetic chicane to stretch the energy modulation, leading to a finely striated pattern in the electron beam. After that the electron beam sequentially interacts with the second seed laser in the second modulator and passes through the second magnetic chicane to generate a significant bunching at high harmonics, where only a small energy modulation is required considering that the slice energy spread in individual striation is relatively small. After passing the second modulator, the beam is density modulated at the wavenumbers given by  $k_a = nk_{seed1} + mk_{seed2}$ , where  $k_{seed1}$  and  $k_{seed2}$  are the wavenumbers of two seed lasers,  $k_{seed1,2} = 2\pi/\lambda_{seed1,2}$ , and  $n, m$  are non-zero integers. Then, we can obtain  $k_a = (n + m)k_s$  and  $\lambda_a = \lambda_s/a$ , where  $\lambda_a = 2\pi/k_a$  and  $a$  is integer  $a = n + m$ . The harmonic up-conversion efficiency of EEHG can be qualified by the bunching factor, which can be calculated by Xiang [23].

$$b_{n,m} = \left| e^{-1/2[nB_1 + (Km+n)B_2]^2} J_m[-(Km+n)A_2B_2] \times J_n\{-A_1[nB_1 + (Km+n)B_2]\} \right| \quad (1)$$

where  $A_{1,2}$  are the energy modulation amplitude divided by the initial energy spread  $\sigma_{E_0}$ ,  $B_{1,2} = R_{56}^{(1,2)}K\sigma_{E_0}$  are the dimensionless dispersion strengths for the two dispersions,  $K = k_{seed2}/k_{seed1} = 1$ .

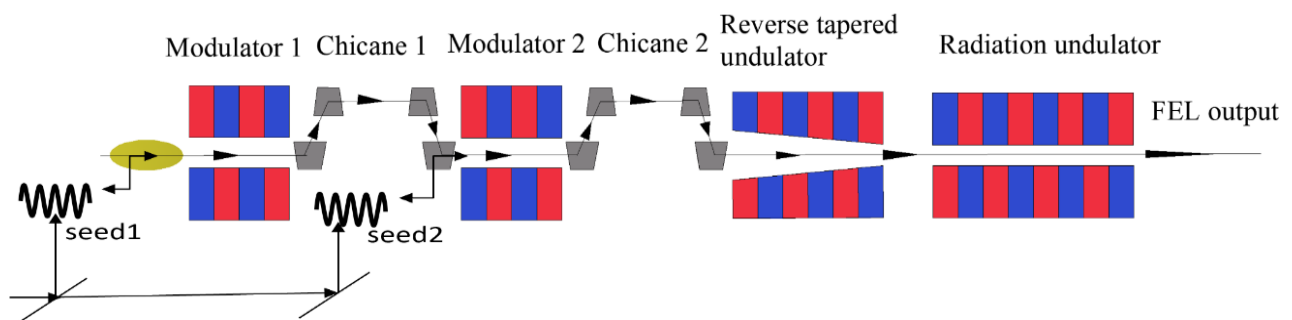


Figure 1. Schematic layout of the reverse taper enhanced harmonic cascade technique.

Afterwards, the electron beam passes through a reverse tapered undulator to enhance the coherent microbunching while suppressing the growth of the energy spread. The reverse taper technique was initially used to increase the saturation efficiency of FEL oscillation [31]. Recently, polarization control in an X-ray FEL has been experimentally demonstrated in LCLS by using reverse taper technique [34]. With an initial bunching factor  $b_a$ , the fundamental bunching factor  $b_a(z)$  and the complex amplitude of energy modulation  $b_p$  in the reverse tapered undulator can be expressed as [33]

$$|b_a(z)|^2 \simeq |\beta \hat{z}|^2 \hat{\eta}, \quad |b_p|^2 \simeq |\beta \hat{z}| \hat{\eta} \tag{2}$$

where  $\beta$  is the taper strength  $\beta = -\frac{\lambda_u}{4\pi\rho^2} \frac{K}{1+K^2} \frac{dK}{dz}$ ,  $\hat{\eta}$  is the normalized FEL power,  $\lambda_u$  is the undulator period,  $\rho$  is FEL pierce parameter, and  $\hat{z} = \frac{4\pi\rho z}{\lambda_u}$  ( $z$  is the distance along the undulator). Due to the non-linear harmonic radiation [36,37], the bunching factor at the  $a_1$ th harmonic of the resonance of EEHG becomes [35]

$$|b_h|^2 \propto A |\beta \hat{z}|^2 \hat{\eta}, \tag{3}$$

where  $A$  is a constant and  $h = aa_1$ . According to Equations (2) and (3), one can find that the bunching factor  $b_h$  is proportional to  $\beta$  while the energy modulation amplitude  $b_p$  is proportional to  $\sqrt{\beta}$ . Compared with the non-tapered undulator, the  $b_h$  varies slowly with  $\beta$  while the power of radiation and energy spread induced by emission are reduced significantly, which means that the quality of the electron beam can be well preserved. The electron beam is extracted when the bunching at higher harmonic  $\lambda_h$  ( $\lambda_h = \lambda_a/a_1$ ,  $a_1$  is the harmonic number) grows sufficient large. Finally, the electron beam passes through the radiator to initiate coherent radiation at a target higher harmonic and further amplify it to saturation.

### 3. Results

#### 3.1. Performance without Three-Dimensional Effects

To illustrate the feasibility of the proposed technique, simulations with MATLAB and GENESIS [38] are carried out using the typical parameters of a soft X-ray FEL, as listed in Table 1. An electron beam with beam energy of 2.5 GeV and bunch length of 100 fs is adopted, and various three-dimensional effects are ignored in this simulation. Specifically, we consider an electron beam with uniform current  $I$ , energy spread  $\sigma_{E_0}$  and normalized transverse emittance  $\varepsilon$  in the longitudinal position. Here, we consider a seed laser with the conventional wavelength of 265 nm [29] and harmonic up-shift numbers of  $a = 75$  and  $a_1 = 3$ . To ensure the seed laser can well modulate the electron beam, the lengths of seed lasers are chosen as 200 fs. The bunching factor in Equation (1) is determined by four parameters  $A_1, A_2, B_1, B_2$ . The optimized values of  $B_1, B_2$  vary by using different combinations of  $n$  and  $m$ , and the optimized value of  $B_1$  is nearly inversely proportional to  $|n|$  [23]. Here, we adopt  $n = -2$  and  $m = 77$  to optimize the bunching factor  $b_{75}$ . The energy modulation amplitudes are  $A_1 = 3.5, A_2 = 2$ , the calculated  $b_{75}$  as a function of  $B_1, B_2$  are shown in Figure 2a, where the optimized values are  $B_1 = 15.75, B_2 = 0.43$ . With these optimized values, the calculated  $b_{75}$  as a function of  $A_1, A_2$  are shown in Figure 2b. The relation between the calculated bunching factor and harmonic number is presented in Figure 2c, where one can find that  $b_{75} = 0.058$ . The bunching factor is optimized at 75th harmonic, therefore  $b_{75}$  is larger than the bunching factor at other harmonics. According to Figure 2, one can find the bunching factor is sensitive to the optimized parameters, therefore there are jumps between different harmonics.

**Table 1.** Main parameters of a soft x-ray free-electron lasers (FEL) facility.

Parameters	Value
Electron beam energy	2.5 GeV
Energy spread	0.005%
Peak current	500 A
Bunch length (rms)	100 fs
Normalized emittance	1 $\mu\text{m}$ -rad
Longitudinal phase space	Uniform
Current profile	Gaussian
Seed laser wavelength (1,2)	265 nm
Reverse tapered undulator period	43 mm
Radiation undulator period	27 mm
Seed laser length	200 fs

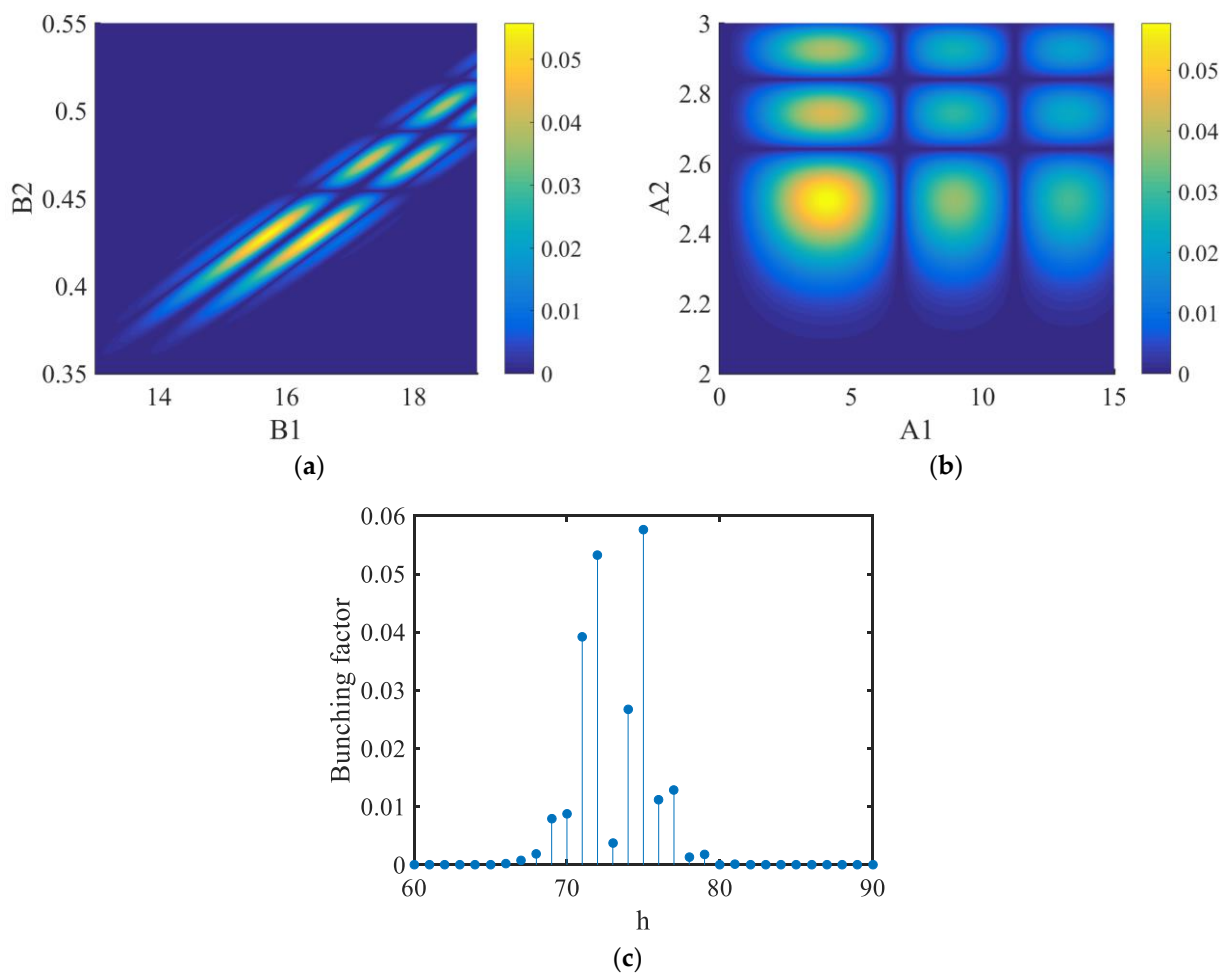


**Figure 2.** (a) The calculated bunching factor at 75th harmonic  $b_{75}$  as a function of  $B_1, B_2$  ( $A_1 = 3.5, A_2 = 2$ ); (b) The calculated bunching factor at 75th harmonic  $b_{75}$  as a function of  $A_1, A_2$  ( $B_1 = 15.75, B_2 = 0.43$ ); (c) The relation between the calculated bunching factors and harmonic numbers  $h$ .

In our simulations, the electron beam is initially generated in GENESIS. Firstly, we ignore 3D effects and perform the modulation processes with a simple 1D algorithm based on MATLAB using the simple equations in Xiang [23]. Simulation results are illustrated in Figure 3. This bunched electron beam is then sent into the reverse tapered undulator resonated at 75th harmonic (3.5 nm) of the seed. The strength of reverse taper  $\beta$  has been tuned to optimize the bunching factor at 225th harmonic and reduce the growth of the electron beam energy spread as well [33]. Simulations for the reverse tapered undulator

and the final radiator are performed with GENESIS. Figure 4 shows the energy spread at saturation  $\sigma_s$  and saturation peak power  $P_s$  as functions of the taper strength  $\beta$ . One can find that the  $\sigma_s$  and  $P_s$  increase with  $\beta$  and the FEL saturation peak power drops quickly when  $\beta$  is negative.

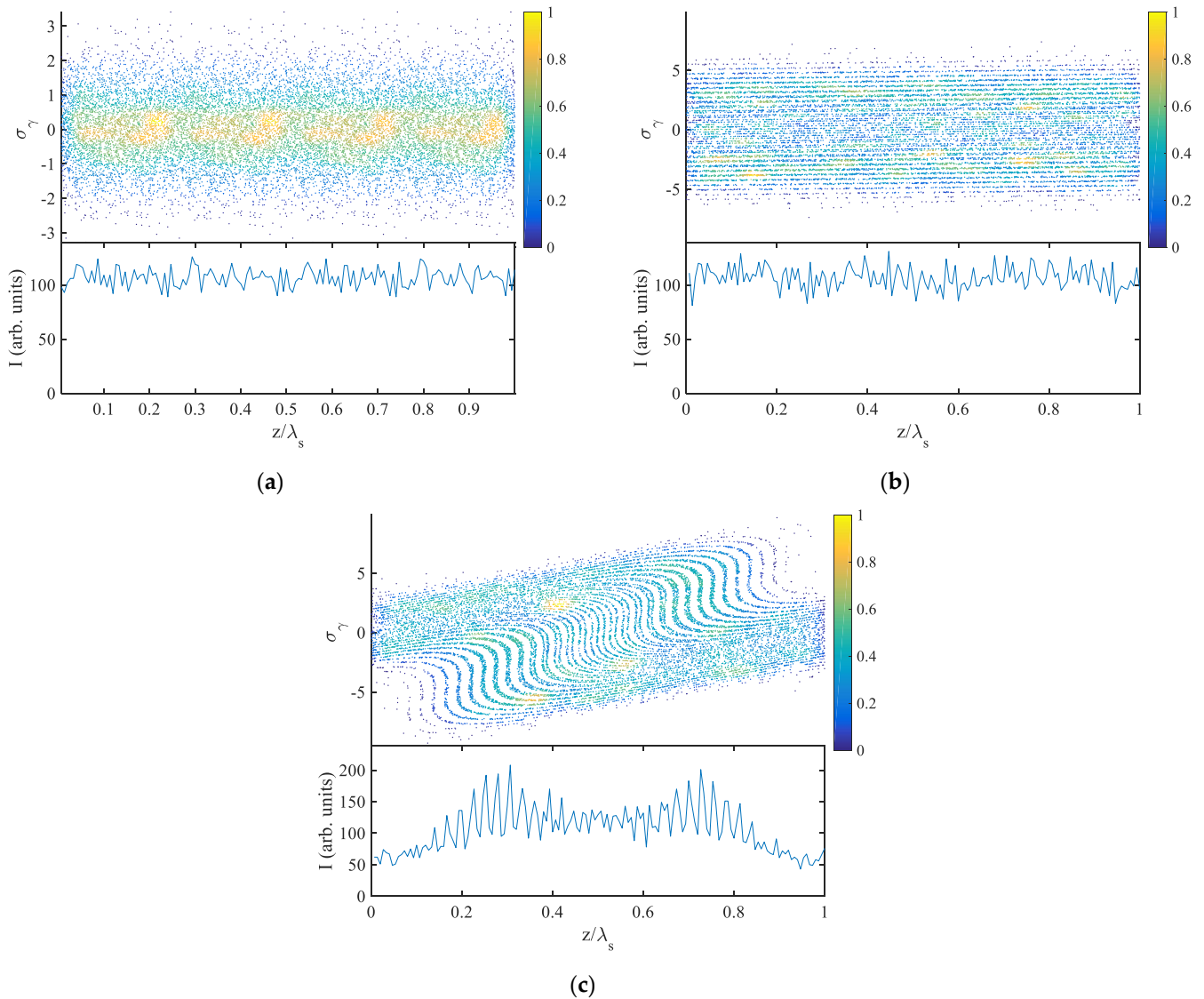


**Figure 3.** The longitudinal phase space and current profile evolutions in EEHG technique. (a) Phase space and current before the modulator 1; (b) Phase space and current at the exit of dispersion 1; (c) Phase space and current at the exit of dispersion 2.

While stronger reverse taper strength can suppress the radiation power better, the detuning effect to the spectrum needs to be considered. Here we adopt the taper strength  $\beta = -0.5$ . The undulator parameter  $K$  at the entrance of undulator is 1.71. The evolutions of FEL peak power, bunching factor at the 225th harmonic (3rd harmonic of the undulator) and the energy spread along the undulator distance for different cases are presented in Figure 5, where one can clearly see that the radiation power and the energy spread are significantly suppressed by the reverse tapered undulator and the bunching factor can grow sufficiently high. The bunching factor at the 225th harmonic should dominate FEL amplification process while keeping the energy spread small in the following radiator. A relatively large bunching factor of 0.1 is chosen considering that the energy spread grows very slowly. The equivalent shot noise seed power can be calculated about 86 W, which

can be easily suppressed by the bunching factor. To achieve a bunching factor of 0.1, the required length for the reverse tapered undulator is about 12.3 m (blue dots in Figure 5), where the electron beam is extracted in our simulation.

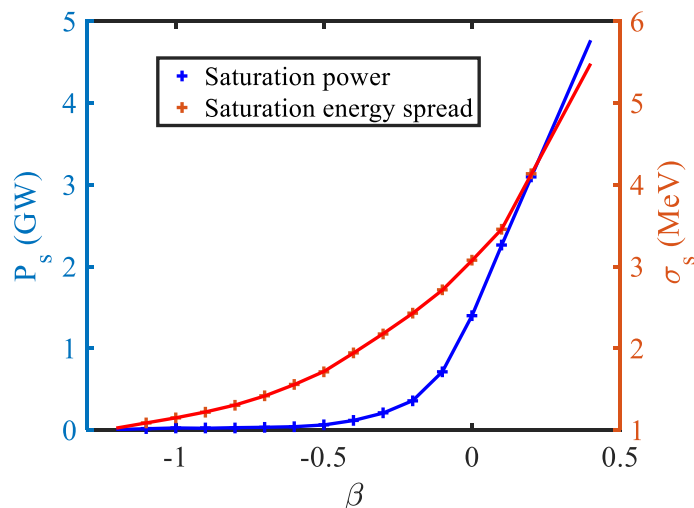


**Figure 4.** The energy spread at saturation  $\sigma_s$  and saturation peak power  $P_s$  as functions of taper strength  $\beta$ . The “crosses” represent the simulation results and the solid lines are the fitting curves.

The bunched electron beam and the radiation pulse from reverse tapered undulator are sent into the radiator to amplify the radiation at 225th harmonic. For comparison, simulations for a single-stage EEHG operated at 225th harmonic have also been performed. As mentioned before, the optimized value of  $B_1$  is nearly inversely proportional to  $|n|$ , the value of  $|n|$  need to be relatively large to reduce the value of  $B_1$  thus reducing various three-dimensional effects. The optimization of  $n$  for ultra-high harmonic have been performed in Zhou [39]. Here, we adopt  $n = -4$  and  $m = 229$  to optimize the bunching factor of EEHG, and the optimized parameters are  $A_1 = 6.1$ ,  $A_2 = 1.05$ ,  $B_1 = 55.48$ ,  $B_2 = 0.99$ . The bunched electron beam from the single-stage EEHG is directly sent into the final radiator. Figure 6a shows the gain curves for different cases. The proposed technique gets saturation with the total undulator (the reverse tapered undulator and the final radiator) length of 30 m (blue lines). The output peak power is about 1 GW. When the taper is tuned to zero, coherent radiation at 225th harmonic cannot be amplified due to large energy spread induced by the undulator (red lines). The single-stage EEHG saturates at about 28 m with an output peak power of 1.8 GW, higher than that achieved by the proposed method due to the smaller energy spread. The normalized spectra at saturation are shown in Figure 6b, where the FWHM (full width at half maximum) spectral bandwidth of the proposed technique is  $1.27 \times 10^{-5}$ , comparable with that from a single-stage EEHG. However, the performance of a single-stage EEHG is very sensitive to various three-dimensional effects such as intra beam scattering (IBS), coherent and incoherent synchrotron radiation (CSR and ISR), leading to the overwhelming of the coherent signal at ultra-high harmonics [23,28].

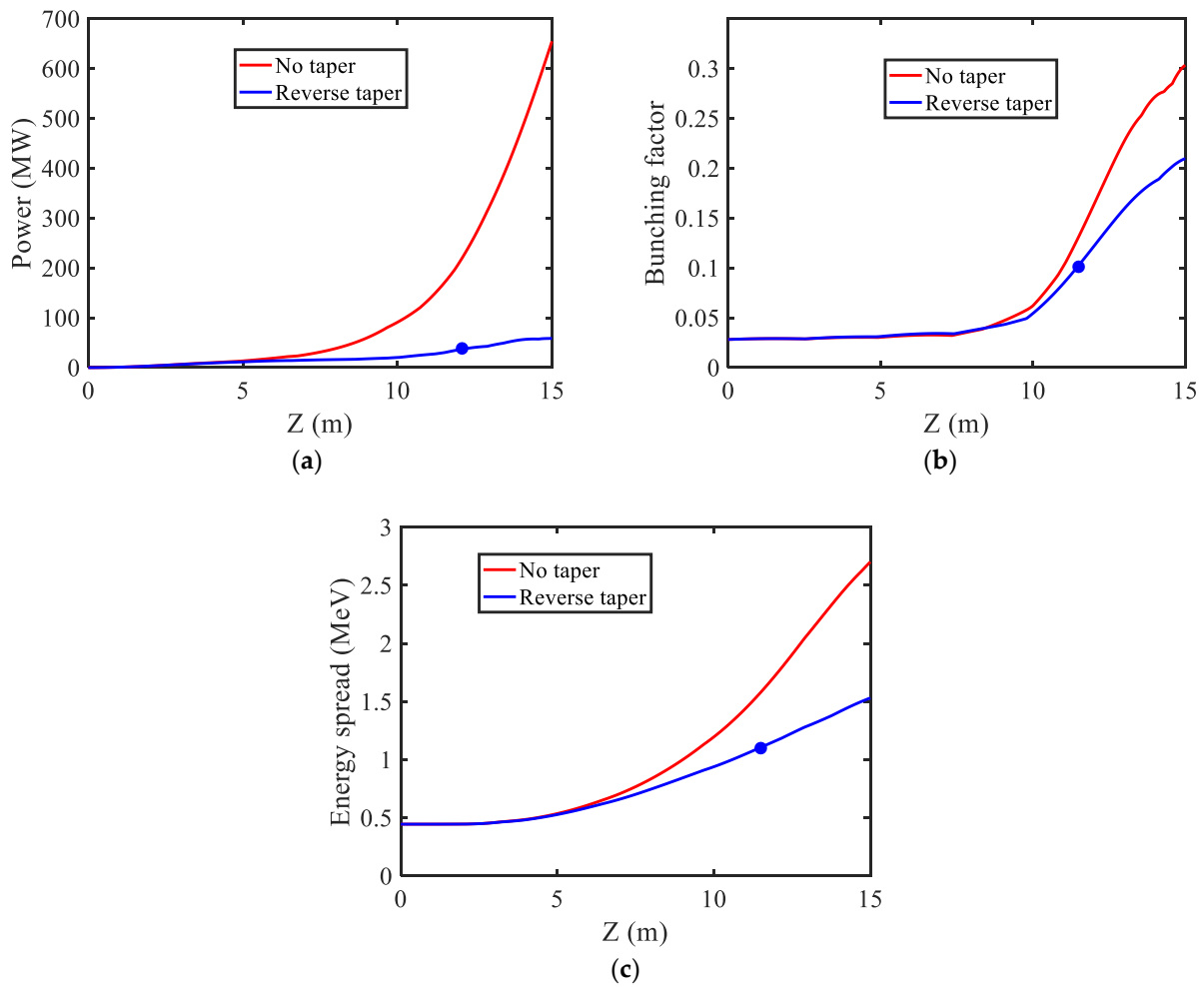


**Figure 5.** The evolutions of FEL peak power (a), bunching factor at the 225th harmonic of the seed (b) and energy spread (c). The red lines represent the case without taper and the blue lines represent the case with reverse taper. The electron beam is extracted from the reverse tapered undulator at the blue point (12.3 m).

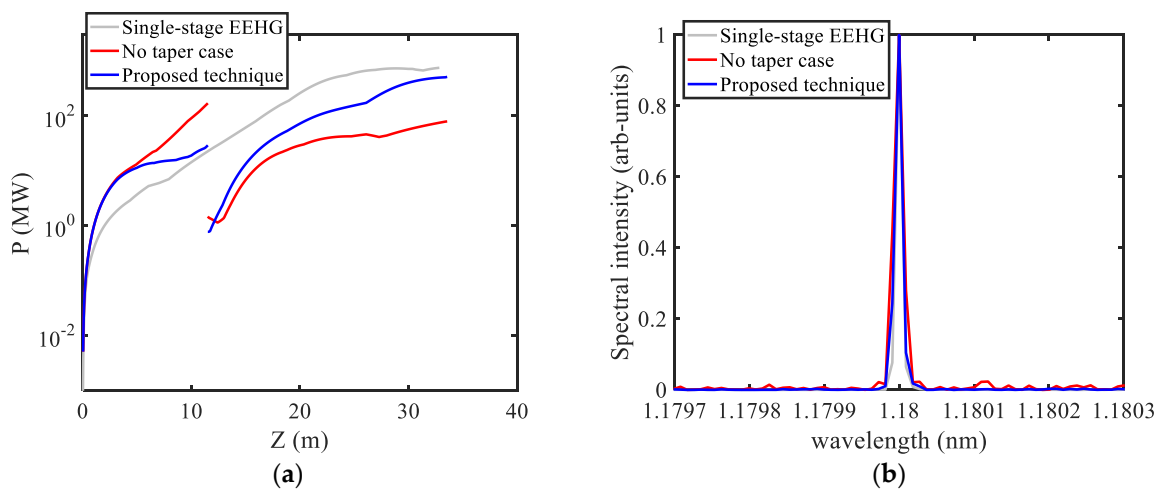


**Figure 6.** (a) The FEL peak power  $P$  evolutions along the undulator (reverse tapered undulator and radiator) for single-stage EEHG (gray), the proposed technique without taper (red) and with reverse taper (blue); (b) The saturation spectra for these three cases.

### 3.2. Performance with Three-Dimensional Effects

The merit of the proposed technique is that it can decrease the harmonic number of EEHG by several times, this can significantly decrease the impact of various three-dimensional effects. The ISR effect of chicane 1 will cause energy diffusion on the energy bands in longitudinal phase space [40–44]. The CSR wake of the chicane 1 can introduce additional energy modulation at long wavelength [45–50]. These effects will result in the damping of the bunching factor and the output coherence at ultra-high harmonics. When the beam with a relativistic energy  $\gamma$  passes through a dipole with a length  $L$ , a bending radius  $R$  and a bending angle  $\theta$ , the ISR induced energy spread can be calculated by Chao [40]

$$\frac{\Delta\sigma_{E,ISR}^2}{E_0^2} = 2.6 \times 10^{-10} E_0(\text{GeV})^5 \frac{1}{R^2(\text{m}^2)} \frac{\theta}{2\pi}. \tag{4}$$

We assume that the chicane 1 has a symmetric four-dipole structure, the length of each dipole is 1 m and the distance between the first two dipoles is 4 m. The distance between the middle two dipoles is 0.5 m. The bending angle is about 2.34 degrees for the proposed technique and 4.39 degrees for single-stage EEHG. The ISR induced energy spread of chicane 1 is calculated as 5.2 keV for the proposed technique and 17 keV for single-stage EEHG. The dispersion strength of chicane 2 is 0.43, which is relatively weak and the ISR induced energy spread is negligible. The length of each dipole in chicane 2 is 0.3 m and the distance between the first two dipoles is 1 m. The distance between the middle two dipoles is 0.5 m. The longitudinal effect of CSR is characterized by the rms induced energy difference in the electron beam, and the CSR-induced relative energy difference can be calculated by Derbenev [48]

$$\Delta E_{CSR} = 0.22 \frac{N\gamma Lmc^2}{R^{2/3}\sigma_b^{4/3}}, \tag{5}$$

where  $N$  is the number of electrons in one bunch,  $\sigma_b$  is the length of the electron beam. The CSR induced energy difference is calculated as 0.83 MeV for the proposed technique and 1.26 MeV for the single-stage EEHG. Figure 7 shows the ISR induced energy spread and CSR induced energy difference as functions of the dispersion strength of chicane 1. With a much weaker chicane 1, the proposed technique can significantly reduce the ISR induced energy spread, and it can also preserve the purity of spectrum by reducing the CSR induced energy difference in the electron beam.

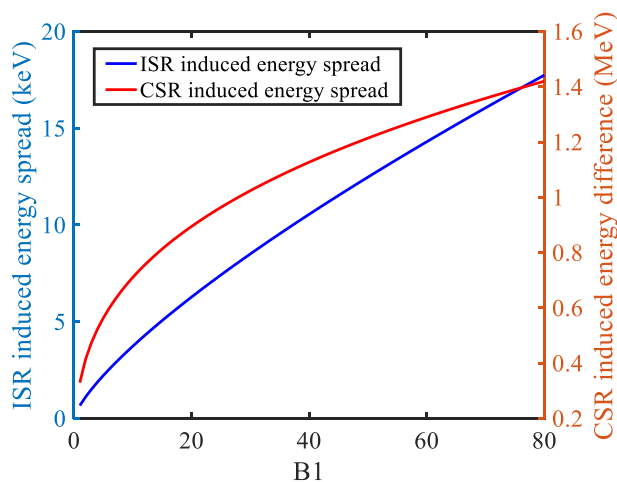


**Figure 7.** The incoherent synchrotron radiation (ISR) induced energy spread (left coordinate, blue) and coherent synchrotron radiation (CSR) induced energy difference (right coordinate, red) as functions of the dispersion strength of chicane 1.

To study the effects of CSR and ISR, simulations are carried out by the combined use of the codes ELEGANT [51] and GENESIS. GENESIS is employed to perform the simulations in the undulators, including the initial beam generation, energy modulation and radiation processes, while the density modulations in the two dispersion chicanes and the beam transport through drift sections and matching quadrupoles are simulated by ELEGANT, taking into account the CSR, ISR and longitudinal space charge effects. In the simulations, 4,637,465 macro-particles are used. The particles are randomly ordered and sampled according to the current profile when going from GENESIS to ELEGANT. When going from ELEGANT to GENESIS, the particles are sliced based on the position in the electron beam and current profile; we have added the particles by copying the nearest particles in the longitudinal position. Figure 8a,b shows the peak power and bunching factor evolutions along the radiator of the proposed technique for different cases. These results indicate that the CSR and ISR have limited impacts on the proposed technique. Figure 8c shows normalized the radiation spectra at saturation. One can find that CSR and ISR effects have induced some sidebands and broaden the FWHM spectral bandwidth of the proposed technique to  $5.08 \times 10^{-5}$ , which is still much narrower than the output FWHM spectral bandwidth of a soft X-ray self-seeding (about  $1 \times 10^{-4}$ ) [52]. For a single-stage EEHG, the coherent signal at 225th harmonic will be totally overwhelmed by the noise induced by CSR and ISR effects, as shown in Figure 8c, where one can observe that the final spectrum becomes a typical SASE structure.

The IBS [53–55] also has significant effects on the bunching factor of EEHG [50]. The IBS effect can be hardly handled in the simulations above. The IBS model for EEHG can be simplified as collisions that occur in a drift section of length  $S$  after the chicane 1, and the distribution function of the electron beam  $f$  satisfies the formula [54]

$$\frac{\partial f}{\partial s} = \frac{1}{2} D \frac{\partial^2 f}{\partial \Delta E^2}, \tag{6}$$

where  $D$  is the diffusion coefficient,  $D = \frac{\pi^{1/2} e^4 \Lambda}{2 \epsilon r_e \sigma_x^2} \frac{I}{I_A}$ ,  $r_e$  is the classical electron radius,  $I_A = mc^3/e$  is the Alfvén current ( $I_A = 17.05kA$ ),  $I$  is the beam current,  $\sigma_x$  is the transverse size of beam,  $\Lambda$  is the coulomb logarithm. In the practical units,  $D = 3.1 \frac{I}{\epsilon_x \sigma_x}$  if assuming  $\Lambda = 8$ . The bunching factor with coulomb collisions can be expressed as a product of the bunching factor without collision  $b_h^{(0)}$  and a suppression factor

$$b_h = b_h^{(0)} e^{-S/L}, \tag{7}$$

where  $L = 2\sigma_{E_0}^2 / Dh^2 B_2^2$ . Figure 9 shows the bunching suppression factors as functions of the drift section length  $S$  for three different harmonics ( $h = 75, h = 150, h = 225$ ). One can find that the bunching factor is very sensitive to the IBS effect when the harmonic number is larger than 100. In this paper, the total length of modulator 2 and chicane 2 is about 4 m, the bunching suppression factor is calculated as about 0.9, which is acceptable for EEHG at 75th harmonic. While for the single-stage EEHG, the bunching suppression factor for a 4 m long transmission section is about 0.3, which will decrease the bunching factor to the shot noise level.

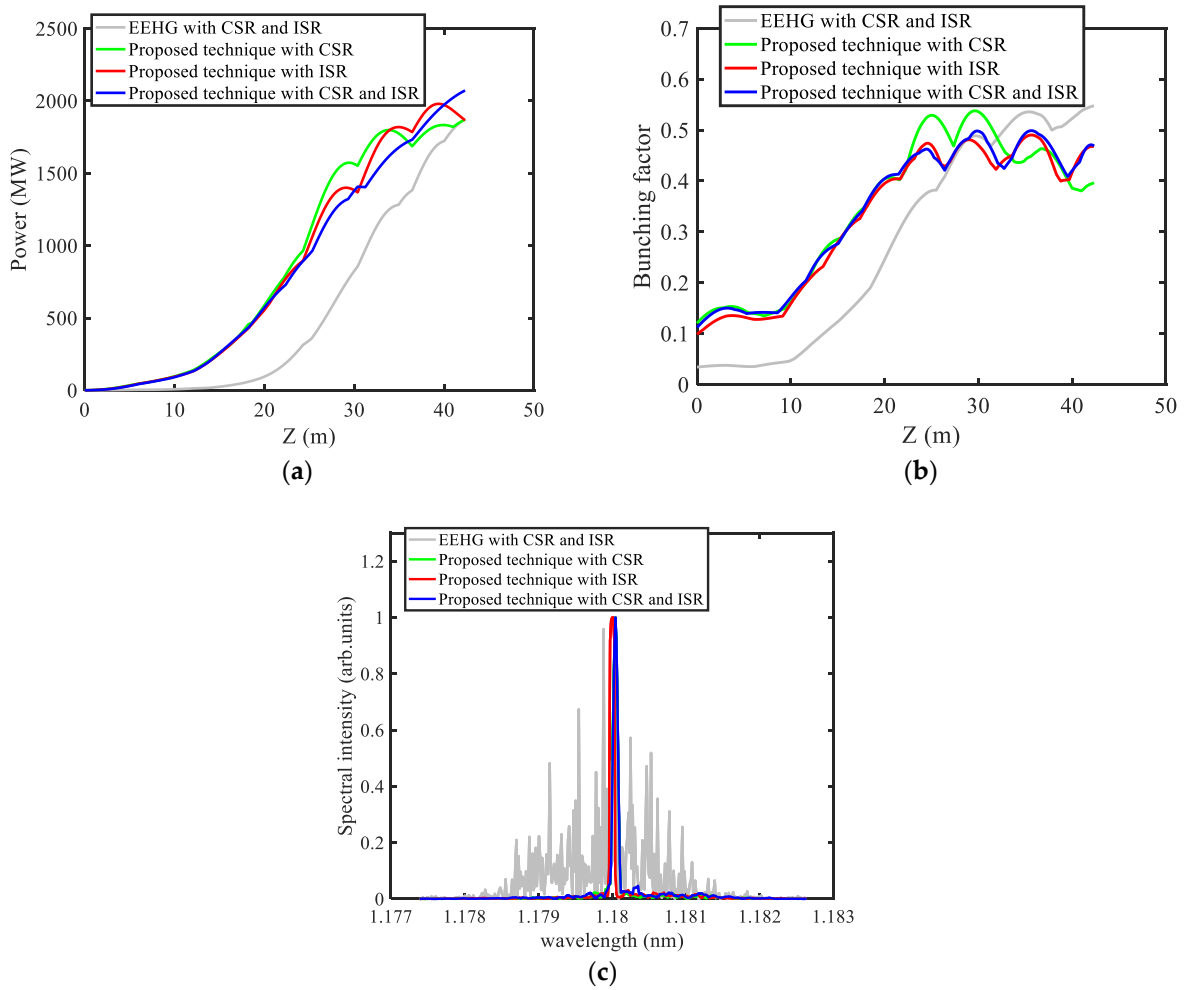


**Figure 8.** The FEL peak power (a) and bunching factor (b) evolutions along the undulator for the four cases: the proposed techniques with CSR (green), with ISR (red), with CSR and ISR (blue) and single-stage EEHG (gray); (c) The radiation spectra at saturation for these cases.

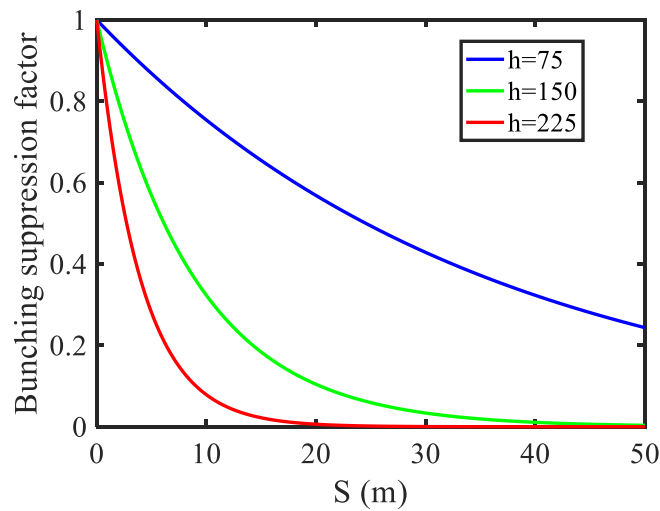


**Figure 9.** The bunching suppression factors as functions of the drift section length  $S$  for three different harmonics ( $h = 75$  (blue),  $h = 150$  (green),  $h = 225$  (red)).

#### 4. Discussion

In this paper, simulations of the proposed technique are performed with and without three-dimensional effects, the results show that the proposed technique can extend the frequency up-conversion efficiency of EEHG and reduce the various three-dimensional effects of beam by radiating at relatively lower harmonic of EEHG. The spectral bandwidth of the proposed technique is narrower than that of a conventional soft X-ray self-seeding [52]. The proposed technique can further extend the photon energy coverage to hard X-ray by increasing the harmonic number, and it also has a relatively simpler configuration than the two-stage seeded FEL [56] while achieving similar FEL radiation. It should be noted that the proposed technique may have some possible issues due to that EEHG and reverse tapered undulator are utilized: firstly, the three-dimensional effects may affect the bunching forming process of EEHG for high charge electron beam; secondly, the optimization of reverse taper parameters may affect the properties of final FEL pulses, these topics would be studied in the future.

#### 5. Conclusions

In summary, a new method is proposed to extend the photon energy coverage of a single-stage seeded FEL by combining the reverse taper technique with the EEHG. Using the typical parameters of a soft X-ray FEL facility, theoretical analysis and numerical simulation demonstrate that the proposed technique can significantly decrease the impact of various three-dimensional effects. The proposed technique is feasible to produce the coherent X-ray radiation at 1 keV with a relatively simple configuration. Therefore, it can reduce the difficulties and requirements in implementing external seeding at sub-nanometer wavelength range.

**Author Contributions:** Conceptualization, C.F. and K.Z.; methodology, K.Z. and C.F.; software, K.Z.; validation, K.Z., T.L. and C.F.; formal analysis, K.Z., Z.Q., X.F.; investigation, K.Z.; data curation, K.Z.; writing—original draft preparation, K.Z.; writing—review and editing, K.Z., C.F., T.L., Z.Q. and X.F.; visualization, K.Z.; supervision, C.F., H.D. and B.L.; project administration, C.F., H.D. and B.L.; funding acquisition, C.F. All authors have read and agreed to the published version of the manuscript.

**Funding:** This research was funded by National Natural Science Foundation of China and Shanghai Municipal Science and Technology Major Project, grant number 11975300 and 2017SHZDZX02.

**Institutional Review Board Statement:** Not applicable.

**Informed Consent Statement:** Not applicable.

**Data Availability Statement:** Data sharing is not applicable to this article.

**Acknowledgments:** The authors would like to thank Xiaohao Dong, Zheng Qi, Li Zeng and Chaoyang Li (Speccreation Co., Ltd.) for helpful discussions and useful comments.

**Conflicts of Interest:** The authors declare no conflict of interest.

#### References

1. Kondratenko, A.M.; Saldin, E.L. Generation of Coherent Radiation by a relativistic Electron Beam in an Undulator. *Part. Accel.* **1980**, *10*, 207–216.
2. Bonifacio, R.; Pellegrini, C.; Narducci, L. Collective instabilities and high-gain regime in a free electron laser. *Opt. Commun.* **1984**, *50*, 373–378. [[CrossRef](#)]
3. Dattoli, G.; Marino, A.; Renieri, A.; Romanelli, F. Progress in the Hamiltonian picture of the free-electron laser. *IEEE J. Quantum Electron.* **1981**, *17*, 1371–1387. [[CrossRef](#)]
4. Colson, W. Tutorial on classical free electron laser theory. *Laser Handb.* **1990**, *6*, 75. [[CrossRef](#)]
5. Andruszkow, J.; Aune, B.; Ayvazyan, V.; Baboi, N.; Bakker, R.; Balakin, V.; Barni, D.; Bazhan, A.; Bernard, M.; Bosotti, A.; et al. First Observation of Self-Amplified Spontaneous Emission in a Free-Electron Laser at 109 nm Wavelength. *Phys. Rev. Lett.* **2000**, *85*, 3825–3829. [[CrossRef](#)]
6. Huang, Z.; Kim, K.-J. Review of x-ray free-electron laser theory. *Phys. Rev. Spec. Top. Accel. Beams* **2007**, *10*, 034801. [[CrossRef](#)]
7. Feng, C.; Deng, H.-X. Review of fully coherent free-electron lasers. *Nucl. Sci. Tech.* **2018**, *29*, 160. [[CrossRef](#)]

8. Hau-Riege, S.P.; Chapman, H.N.; Krzywinski, J.; Sobierajski, R.; Bajt, S.; London, R.A.; Bergh, M.; Caleman, C.; Nietubyc, R.; Juha, L.; et al. Subnanometer-Scale Measurements of the Interaction of Ultrafast Soft X-Ray Free-Electron-Laser Pulses with Matter. *Phys. Rev. Lett.* **2007**, *98*, 145502. [[CrossRef](#)]
9. Young, L.; Kanter, E.P.; Krässig, B.; Li, Y.; March, A.M.; Pratt, S.T.; Santra, R.; Southworth, S.H.; Rohringer, N.; DiMauro, L.F.; et al. Femtosecond electronic response of atoms to ultra-intense X-rays. *Nat. Cell Biol.* **2010**, *466*, 56–61. [[CrossRef](#)]
10. Inoue, I.; Osaka, T.; Hara, T.; Tanaka, T.; Inagaki, T.; Fukui, T.; Goto, S.; Inubushi, Y.; Kimura, H.; Kinjo, R.; et al. Generation of narrow-band X-ray free-electron laser via reflection self-seeding. *Nat. Photonics* **2019**, *13*, 319–322. [[CrossRef](#)]
11. Feldhaus, J.; Saldin, E.L.; Schneider, J.R.; Schneidmiller, E.A.; Yurkov, M.V. Possible application of X-ray optical elements for reducing the spectral bandwidth of an X-ray SASE FEL. *Opt. Commun.* **1997**, *140*, 341–352. [[CrossRef](#)]
12. Feng, Y.; Amann, J.; Cocco, D.; Field, C.; Hastings, J.; Heimann, P.; Huang, Z.; Loos, H.; Welch, J.; Wu, J.; et al. System Design for self-seeding the LCLS at Soft X-ray energies. In Proceedings of the 24th International FEL Conference, Nara, Japan, 26–31 August 2012.
13. Stoupin, S.; Blank, V.; Terentyev, S.; Polyakov, S.; Denisov, V.; Kuznetsov, M.; Shvyd'Ko, Y.; Shu, D.; Emma, P.; Maj, J.; et al. Diamond crystal optics for self-seeding of hard X-rays in X-ray free-electron lasers. *Diam. Relat. Mater.* **2013**, *33*, 1–4. [[CrossRef](#)]
14. Zhang, K.; Qi, Z.; Feng, C.; Deng, H.; Wang, D.; Zhao, Z. Extending the photon energy coverage of an x-ray self-seeding FEL via the re-verse taper enhanced harmonic generation technique. *Nucl. Instrum. Methods A* **2017**, *854*, 3–10. [[CrossRef](#)]
15. Emma, C.; Lutman, A.; Guetg, M.; Krzywinski, J.; Marinelli, A.; Wu, J.; Pellegrini, C. Experimental demonstration of fresh bunch self-seeding in an X-ray free electron laser. *Appl. Phys. Lett.* **2017**, *110*, 154101. [[CrossRef](#)]
16. Ratner, D.; Abela, R.; Amann, J.; Behrens, C.; Bohler, D.; Bouchard, G.; Bostedt, C.; Boyes, M.; Chow, K.; Cocco, D.; et al. Experimental Demonstration of a Soft X-Ray Self-Seeded Free-Electron Laser. *Phys. Rev. Lett.* **2015**, *114*, 054801. [[CrossRef](#)]
17. Amann, J.; Berg, W.J.; Blank, V.D.; Decker, F.-J.; Ding, Y.; Emma, P.; Feng, Y.; Frisch, J.; Fritz, D.M.; Hastings, J.B.; et al. Demonstration of self-seeding in a hard-X-ray free-electron laser. *Nat. Photonics* **2012**, *6*, 693–698. [[CrossRef](#)]
18. Yu, L.H. Generation of intense uv radiation by subharmonically seeded single-pass free-electron lasers. *Phys. Rev. A* **1991**, *44*, 5178–5193. [[CrossRef](#)]
19. Yu, L.; Di Mauro, L.; Doyuran, A.; Graves, W.S.; Johnson, E.D.; Heese, R.; Krinsky, S.; Loos, H.; Murphy, J.B.; Rakowsky, G.; et al. First Ultraviolet High-Gain Harmonic-Generation Free-Electron Laser. *Phys. Rev. Lett.* **2003**, *91*, 074801. [[CrossRef](#)]
20. Deng, H.; Dai, Z. Harmonic lasing of X-ray free electron laser: On the way to smaller and cheaper. *Chin. Phys. C* **2013**, *37*, 102001. [[CrossRef](#)]
21. Feng, C.; Zhang, M.; Lin, G.; Gu, Q.; Deng, H.-X.; Chen, J.; Wang, D.; Zhao, Z. Design study for the cascaded HGHG experiment based on the SDUV-FEL. *Chin. Sci. Bull.* **2012**, *57*, 3423–3429. [[CrossRef](#)]
22. Dattoli, G.; Ottaviani, P.L. Design considerations for x-ray free electron lasers. *J. Appl. Phys.* **1999**, *86*, 5331–5336. [[CrossRef](#)]
23. Xiang, D.; Stupakov, G. Echo-enabled harmonic generation free electron laser. *Phys. Rev. Spec. Top. Accel. Beams* **2009**, *12*, 030702. [[CrossRef](#)]
24. Zhao, Z.T.; Wang, D.; Chen, J.H.; Chen, Z.H.; Deng, H.X.; Ding, J.G.; Feng, C.; Gu, Q.; Huang, M.M.; Lan, T.; et al. First lasing of an echo-enabled harmonic generation free-electron laser. *Nat. Photonics* **2012**, *6*, 360–363. [[CrossRef](#)]
25. Xiang, D.; Colby, E.; Dunning, M.; Gilevich, S.; Hast, C.; Jobe, K.; McCormick, D.; Nelson, J.; Raubenheimer, T.O.; Soong, K.; et al. Evidence of High Harmonics from Echo-Enabled Harmonic Generation for Seeding X-Ray Free Electron Lasers. *Phys. Rev. Lett.* **2012**, *108*, 024802. [[CrossRef](#)] [[PubMed](#)]
26. Hemsing, E.; Dunning, M.; Hast, C.; Raubenheimer, T.O.; Weathersby, S.; Xiang, D. Highly coherent vacuum ultraviolet radiation at the 15th harmonic with echo-enabled harmonic generation technique. *Phys. Rev. Spec. Top. Accel. Beams* **2014**, *17*, 070702. [[CrossRef](#)]
27. Hemsing, E.; Dunning, M.; Garcia, B.; Hast, C.; Raubenheimer, T.; Stupakov, G.; Xiang, D. Echo-enabled harmonics up to the 75th order from precisely tailored electron beams. *Nat. Photonics* **2016**, *10*, 512–515. [[CrossRef](#)]
28. Ribič, P.R.; Abrami, A.; Badano, L.; Bossi, M.; Braun, H.-H.; Bruchon, N.; Capotondi, F.; Castronovo, D.; Cautero, M.; Cinquegrana, P.; et al. Coherent soft X-ray pulses from an echo-enabled harmonic generation free-electron laser. *Nat. Photonics* **2019**, *13*, 555–561. [[CrossRef](#)]
29. Feng, C.; Deng, H.; Zhang, M.; Wang, X.; Chen, S.; Liu, T.; Zhou, K.; Gu, D.; Wang, Z.; Jiang, Z.; et al. Coherent extreme ultraviolet free-electron laser with echo-enabled harmonic generation. *Phys. Rev. Accel. Beams* **2019**, *22*, 050703. [[CrossRef](#)]
30. Rebernik, P.; Roussel, E.; Penn, G.; De Ninno, G.; Giannessi, L.; Penco, G.; Allaria, E. Echo-Enabled Harmonic Generation Studies for the FERMI Free-Electron Laser. *Photonics* **2017**, *4*, 19. [[CrossRef](#)]
31. Saldin, E.; Schneidmiller, E.; Yurkov, M. The features of an FEL oscillator with a tapered undulator. *Opt. Commun.* **1993**, *103*, 297–306. [[CrossRef](#)]
32. Saldin, E.; Schneidmiller, E.; Yurkov, M.V. Self-amplified spontaneous emission FEL with energy-chirped electron beam and its application for generation of attosecond x-ray pulses. *Phys. Rev. Spec. Top. Accel. Beams* **2006**, *9*, 050702. [[CrossRef](#)]
33. Schneidmiller, E.; Yurkov, M.V. Obtaining high degree of circular polarization at x-ray free electron lasers via a reverse undulator taper. *Phys. Rev. Spec. Top. Accel. Beams* **2013**, *16*, 110702. [[CrossRef](#)]
34. Lutman, A.A.; MacArthur, J.P.; Ilchen, M.; Lindahl, A.O.; Buck, J.; Coffee, R.N.; Dakovski, G.L.; Dammann, L.; Ding, Y.; Dürr, H.A.; et al. Polarization control in an X-ray free-electron laser. *Nat. Photonics* **2016**, *10*, 468–472. [[CrossRef](#)]

35. Zhang, K.; Liu, T.; Feng, C. Reverse taper enhanced harmonic lasing for seeding an X-ray free-electron laser. *Nucl. Instrum. Methods A* **2021**, *988*, 164931. [[CrossRef](#)]
36. Colson, W.B. Free-electron lasers operating in higher harmonics. *Phys. Rev. A* **1981**, *24*, 639–641. [[CrossRef](#)]
37. Freund, H.; Biedron, S.; Milton, S. Nonlinear harmonic generation in free-electron lasers. *IEEE J. Quantum Electron.* **2000**, *36*, 275–281. [[CrossRef](#)]
38. Reiche, S. GENESIS 1.3: A fully 3D time-dependent FEL simulation code. *Nucl. Instrum. Methods A* **1999**, *429*, 243–248. [[CrossRef](#)]
39. Zhou, K.; Feng, C.; Wang, D. Feasibility study of generating ultra-high harmonic radiation with a single stage echo-enabled harmonic generation scheme. *Nucl. Instrum. A* **2016**, *834*, 30–35. [[CrossRef](#)]
40. Chao, A.W.; Tigner, M. *Handbook of Accelerator Physics and Engineering*; World Scientific: Singapore, 2006.
41. Xiang, D.; Stupakov, G. Tolerance study for the echo-enabled harmonic generation free electron laser. In Proceedings of the IPAC, Vancouver, BC, Canada, 4–8 May 2009.
42. Douglas, D.R.; Benson, S.V.; Hutton, A. Hutton. Control of Coherent Synchrotron Radiation and Micro-Bunching Effects during Transport of High Brightness Electron Beams. *JLAB-ACP* **2014**, *1751*, 1–27.
43. Marinelli, A.; Pellegrini, C.; Giannessi, L.; Reiche, S. Comparative study of nonideal beam effects in high gain harmonic generation and Self-seeded free electron lasers. *Phys. Rev. Accel. Beams* **2010**, *13*, 070701. [[CrossRef](#)]
44. Douglas, D.; Benson, S.; Hofler, A. Control of Synchrotron Radiation Effects during Recirculation. In Proceedings of the IPAC 2015, Richmond, VA, USA, 3–8 May 2015.
45. Mitri, S.D. Coherent Synchrotron Radiation and Microbunching Instability. *CERN Yellow Rep. Sch. Proc.* **2018**, *1*, 381–400.
46. Heifets, S.; Stupakov, G.; Krinsky, S. Coherent synchrotron radiation instability in a bunch compressor. *Phys. Rev. Accel. Beams* **2002**, *5*, 064401. [[CrossRef](#)]
47. Stupakov, G.; Heifets, S. Beam instability and microbunching due to coherent synchrotron radiation. *Phys. Rev. Spec. Top. Accel. Beams* **2002**, *5*, 054402. [[CrossRef](#)]
48. Derbenev, Y.S.; Saldin, E.L.; Shiltsev, V.D.; Rossbach, J. Microbunch Radiative Tail-Head Interaction. *DESY Notkes-Trasse* **1995**, *85*, 22603.
49. Lou, W.; Hoffstaetter, G.H. Coherent synchrotron radiation wake expressions with two bending magnets and simulation results for a multiturn energy-recovery linac. *Phys. Rev. Accel. Beams* **2020**, *23*, 054404. [[CrossRef](#)]
50. Huang, Z.; Borland, M.; Emma, P.; Kim, K.J. Theory and Simulation of CSR Microbunching in Bunch Compressors. *SLAC-PUB* **2002**, *507*, 318–322.
51. Borland, M. *Elegant: A Flexible SDDS-Compliant Code for Accelerator Simulation*; Argonne National Lab.: Lemont, IL, USA, 2000.
52. Hemsing, E.; Marcus, G.; Fawley, W.M.; Schoenlein, R.W.; Coffee, R.; Dakovski, G.; Hastings, J.; Huang, Z.; Ratner, D.; Raubenheimer, T.; et al. Soft x-ray seeding studies for the SLAC Linac Coherent Light Source II. *Phys. Rev. Accel. Beams* **2019**, *22*, 110701. [[CrossRef](#)]
53. Farley, D.T. The effect of Coulomb collisions on incoherent scattering of radio waves by a plasma. *J. Geophys. Res. Space Phys.* **1964**, *69*, 197–200. [[CrossRef](#)]
54. Stupakov, G. Effect of Coulomb Collisions on Echo-enabled Harmonic Generation (EEHG). In Proceedings of the 33rd International Free Electron Laser Conference, Shanghai, China, 22–26 August 2011.
55. Huang, Z. *Intrabeam Scattering in an X-ray FEL Driver*; SLAC National Accelerator Lab.: Menlo Park, CA, USA, 2018.
56. Zhao, Z.; Feng, C.; Zhang, K.-Q. Two-stage EEHG for coherent hard X-ray generation based on a superconducting linac. *Nucl. Sci. Technol.* **2017**, *28*, 117. [[CrossRef](#)]